

Wannier interpolation of spin accumulation coefficient

Atsuo Shitade¹ and Emi Minamitani^{1,2}

¹*Institute of Scientific and Industrial Research, Osaka University, Ibaraki, Osaka 567-0047, Japan*

²*Japan Science and Technology Agency, PRESTO, Kawaguchi, Saitama 332-0012, Japan*

(Dated: February 10, 2025)

The spin Hall (SH) effect is widely understood as a phenomenon in which spin current flows perpendicular to an electric field. In the presence of a spin-orbit coupling, however, spin current is ambiguous, and the SH conductivity depends on the definition of spin current. In this article, we develop an *ab initio* computational scheme for the spin accumulation coefficient, which characterizes the spin accumulation and would be an alternative indicator of the SH effect. The proposed method has been implemented into an open-source software Wannier90 and serves high-precision *ab initio* research on the SH effect.

I. INTRODUCTION

Spintronics is a research field to exploit the spin degree of freedom of electrons for next-generation devices with high-speed processing and low energy consumption. Spin can be generated electrically even in nonmagnetic systems via spin-orbit couplings (SOCs). One of such phenomena is the spin Hall (SH) effect in which spin current flows perpendicular to an applied electric field and turns into the spin accumulation at the surface [1]. Since the experimental observations in semiconductors [2, 3], the research on the SH effect has been extending to various materials with large SOCs such as heavy metals [1], transition metal dichalcogenides (TMDCs) [4], and anti-ferromagnets [5].

The SH conductivity, namely, the response of spin current to an electric field, has been widely evaluated as an indicator of the SH effect. However, in the presence of SOCs, spin is not conserved, and spin current is ambiguous. The conventional spin current $\hat{J}_{sa}^i = \{\hat{s}_a, \hat{v}^i\}/2$, in which $\hat{s}_a = (\hbar/2)\sigma_a$ and \hat{v}^i are the spin operator with the Pauli matrix σ_a and velocity operator, respectively, has been chosen in most of the literature [6, 7] but suffers some critical problems such as the equilibrium spin current and the absence of a conjugate force, as discussed more in Sec. III A. Instead, we may choose the conserved spin current consisting of the conventional one and spin torque dipole moment [8], leading to a different value of the SH conductivity [9]. There is no guiding principle what definition of spin current should be chosen.

Spin is well defined in contrast to spin current, and the spin accumulation at the surface has been experimentally observed [2, 3]. For the Rashba model with nonmagnetic disorder, the spatial distribution of the spin density was numerically computed by solving the coupled diffusion equations [10–13] or the Landauer-Keldysh formalism [14–16]. In this system, the spin accumulation does occur, while the SH conductivities of both the conventional [10, 17–22] and conserved spin current [23] vanish. These results indicate that spin, rather than spin current, is the primary object. However, it is difficult to compute the spin accumulation for real materials because we need to impose the open boundary conditions or attach the

leads, apply a voltage, and deal with disorder.

In this article, we develop an *ab initio* computational scheme for the spin accumulation coefficient (SAC), namely, the response of spin to an electric field gradient [24–26]. The SAC characterizes the spin accumulation at the surface owing to the SH effect but, counterintuitively, can be evaluated as a bulk property using Bloch wavefunctions. Hence, the SAC would be an alternative indicator of the SH effect. With the help of maximally localized Wannier functions [27] implemented in an open-source software Wannier90 [28], we can evaluate the SAC with high precision for real materials. We apply our method to monolayer TMDC MoS₂ and trigonal tellurium to confirm the consistency with the point group symmetry and the gauge invariance regarding Wannier functions. The SAC is not correlated with the SH conductivity and free from the critical problems of spin current. Our work contributes to quantitative materials research on the SH effect based on solid foundations.

II. RESULTS

A. Wannier interpolation of SAC

We consider the response of spin to an electric field gradient, $\langle \Delta \hat{s}_a \rangle = g_{sa}^{ij} \partial_{x^i} E_j$. Within the relaxation time approximation, the SAC can be evaluated using Bloch wavefunctions as $g_{sa}^{ij} = -\tau \gamma_{sa}^{ij}$ with [25]

$$\gamma_{sa}^{ij} = -\frac{e}{\hbar} \sum_n \int \frac{d^3k}{(2\pi)^3} [-f'(\epsilon_n(\mathbf{k}))] \times [s_{na}^i(\mathbf{k}) \partial_{k_j} \epsilon_n(\mathbf{k}) - s_{na}(\mathbf{k}) \epsilon^{ijk} m_{nk}(\mathbf{k})], \quad (1)$$

in which τ is the phenomenological relaxation time, $-e$ is the elementary charge, and $f(\epsilon) = [e^{(\epsilon-\mu)/k_B T} + 1]^{-1}$ is the Fermi distribution function at the chemical potential μ and temperature T .

$$s_{na}^i(\mathbf{k}) = \frac{i}{2} \langle u_n(\mathbf{k}) | \hat{s}_a \hat{Q}_n(\mathbf{k}) | \partial_{k_i} u_n(\mathbf{k}) \rangle + \text{c.c.}, \quad (2a)$$

$$s_{na}(\mathbf{k}) = \langle u_n(\mathbf{k}) | \hat{s}_a | u_n(\mathbf{k}) \rangle, \quad (2b)$$

$$\epsilon^{ijk} m_{nk}(\mathbf{k}) = \frac{-i}{2} \langle \partial_{k_i} u_n(\mathbf{k}) | [\epsilon_n(\mathbf{k}) - \hat{H}(\mathbf{k})] | \partial_{k_j} u_n(\mathbf{k}) \rangle$$

$$+ \text{c.c.}, \quad (2c)$$

are the spin magnetic quadrupole moment [29], spin polarization, and orbital magnetic moment [30, 31], respectively, in which $\hat{Q}_n(\mathbf{k}) = 1 - |u_n(\mathbf{k})\rangle\langle u_n(\mathbf{k})|$, and $\epsilon_n(\mathbf{k})$ and $|u_n(\mathbf{k})\rangle$ are the eigenvalues and eigenstates of the Bloch Hamiltonian $\hat{H}(\mathbf{k})$. γ_{sa}^{ij} has the same tensor structure and dimension as the SH conductivity.

To evaluate Eq. (2a) in the scheme of Wannier functions, we introduce the trace formula of the spin magnetic quadrupole moment as

$$Q_a^i(\mathbf{k}) = \text{Tr}[\hat{s}_a \hat{Q}(\mathbf{k}) \partial_{k_i} \hat{P}(\mathbf{k})]. \quad (3)$$

Here, $\hat{P}(\mathbf{k}) = |u(\mathbf{k})\rangle\langle u(\mathbf{k})|$ is the projection operator to the occupied subspace, and $\hat{Q}(\mathbf{k}) = 1 - \hat{P}(\mathbf{k})$. We have two gauge choices for a set of Bloch wavefunctions $|u(\mathbf{k})\rangle$. One is the Wannier gauge that is the Fourier transform of Wannier functions, denoted by $|u^{(w)}(\mathbf{k})\rangle$. The other is the Hamiltonian gauge that diagonalizes $\mathbb{H}^{(w)}(\mathbf{k}) = \langle u^{(w)}(\mathbf{k}) | \hat{H}(\mathbf{k}) | u^{(w)}(\mathbf{k}) \rangle$, denoted by $|u^{(h)}(\mathbf{k})\rangle$. Hereafter, a gauge choice is not specified unless explicitly shown. In the Hamiltonian gauge, $f(\mathbf{k})$ is a diagonal matrix with $f_n^{(h)}(\mathbf{k}) = 0, 1$. We also define the projection operator to the Wannier subspace as $\hat{\mathbb{P}}(\mathbf{k}) = |u(\mathbf{k})\rangle\langle u(\mathbf{k})|$ and $\hat{\mathbb{Q}}(\mathbf{k}) = \mathbb{I} - \hat{\mathbb{P}}(\mathbf{k})$, which is related by $\hat{Q}(\mathbf{k}) = \hat{\mathbb{Q}}(\mathbf{k}) + \hat{Q}_{\text{in}}(\mathbf{k})$ with $\hat{Q}_{\text{in}}(\mathbf{k}) = |u(\mathbf{k})\rangle g(\mathbf{k}) \langle u(\mathbf{k})|$ ($f(\mathbf{k}) + g(\mathbf{k}) = 1$). Equation (3) expressed by uppercase Tr, which means trace over the full Hilbert space, is gauge invariant by construction.

Next, to compute Eq. (3) efficiently, we rewrite Eq. (3) using Wannier matrix elements defined only in the Wannier subspace. Following Ref. [32] for the Berry curvature and orbital magnetic moment, we obtain

$$Q_a^i(\mathbf{k}) = \text{tr}[\tilde{Q}_a^i(\mathbf{k}) f(\mathbf{k}) + i \mathbb{S}_a(\mathbf{k}) g(\mathbf{k}) \tilde{\partial}_{k_i} f(\mathbf{k})], \quad (4)$$

in which

$$\tilde{Q}_a^i(\mathbf{k}) = i \langle u(\mathbf{k}) | \hat{s}_a \hat{Q}(\mathbf{k}) | \partial_{k_i} u(\mathbf{k}) \rangle, \quad (5a)$$

$$\mathbb{S}_a(\mathbf{k}) = \langle u(\mathbf{k}) | \hat{s}_a | u(\mathbf{k}) \rangle, \quad (5b)$$

$$\tilde{\partial}_{k_i} f(\mathbf{k}) = \partial_{k_i} f(\mathbf{k}) - i [\mathbb{A}^i(\mathbf{k}), f(\mathbf{k})], \quad (5c)$$

with $\mathbb{A}^i(\mathbf{k}) = i \langle u(\mathbf{k}) | \partial_{k_i} u(\mathbf{k}) \rangle$. These quantities are gauge covariant, namely, transform as $X^{(h)}(\mathbf{k}) = U^\dagger(\mathbf{k}) X^{(w)}(\mathbf{k}) U(\mathbf{k})$ under a gauge transformation $|u^{(h)}(\mathbf{k})\rangle = |u^{(w)}(\mathbf{k})\rangle U(\mathbf{k})$. As a result, Eq. (4) expressed by lowercase tr, which means trace over the Wannier subspace, is also gauge invariant.

Finally, we arrive at

$$Q_a^i(\mathbf{k}) = \text{tr}[Q_a^i(\mathbf{k}) f(\mathbf{k}) - \mathbb{S}_a(\mathbf{k}) \mathbb{A}^i(\mathbf{k}) f(\mathbf{k}) + i \mathbb{S}_a(\mathbf{k}) g(\mathbf{k}) \partial_{k_i} f(\mathbf{k})], \quad (6)$$

using $\tilde{Q}_a^i(\mathbf{k}) = Q_a^i(\mathbf{k}) - \mathbb{S}_a(\mathbf{k}) \mathbb{A}^i(\mathbf{k})$. Here, $Q_a^i(\mathbf{k}) = i \langle u(\mathbf{k}) | \hat{s}_a | \partial_{k_i} u(\mathbf{k}) \rangle$ as well as $\mathbb{S}_a(\mathbf{k})$ and $\mathbb{A}^i(\mathbf{k})$ is computed in Wannier90 from *ab initio* calculations. In the

Hamiltonian gauge, $\partial_{k_i} f^{(h)}(\mathbf{k})$ in Eq. (6) is assumed to be zero, and then we find

$$\sum_n s_{na}^{(h)i}(\mathbf{k}) f_n^{(h)}(\mathbf{k}) = \text{Re } Q_a^i(\mathbf{k}). \quad (7)$$

The trace formula gives a part of the bulk spin magnetic quadrupole moment [29], which is allowed in magnetoelectric materials without either inversion or time-reversal symmetry.

Following Ref. [33] for the Berry curvature and orbital magnetic moment, we obtain Eq. (2a) for the n -th band by choosing fake occupations, namely, $f_{m;n}^{(h)}(\mathbf{k}) = \delta_{mn}$ for given n . Now we are ready to compute the SAC for real materials.

B. Example: monolayer MoS₂

Here we apply our Wannier interpolation of the SAC to two different materials. One example is monolayer TMDC MoS₂. TMDCs are layered materials with a chemical formula of MX_2 , in which M and X are transition metal and chalcogen atoms, respectively. The layers are weakly coupled to each other by the van der Waals (vdW) interaction. In particular, monolayer systems have attracted much attention from the viewpoints of spintronics and valleytronics, and were studied in terms of the SH conductivity [34].

Figure 1(a) shows the Fermi-energy dependence of the SAC per layer. See Sec. IV A for computational details. In this material, the D_{3h} point group symmetry allows the form of $\gamma_{sa}^{ij} = \gamma_1 \epsilon_{1a}^{ij}$, in which ϵ_{1a}^{ij} is a tensor whose nonzero components are $\epsilon_{1z}^{xy} = -\epsilon_{1z}^{yx} = 1$. The negligible error indicates that the computed SAC is consistent with this symmetry. We also check the gauge invariance of the SAC by changing the number of iterations for wannierization. These results validate our implementation.

For comparison, we also show the Fermi-energy dependence of the SH conductivity σ_{sa}^{ij} of the conventional spin current [34] in Fig. 1(b). $\sigma_{sa}^{ij} = \sigma_1 \epsilon_a^{ij}$ is allowed by the symmetry. In general, the SAC and SH conductivity are independent of each other. Right below the Fermi energy painted in purple, where the spin splitting occurs at the K and K' points owing to the Ising SOC, the SAC shows a positive plateau, while the SH conductivity shows negative increase. Such a plateau in the SAC can be detected in experiments by changing the carrier density.

C. Example: trigonal tellurium

The other example is trigonal tellurium, in which the nonlinear Hall effect [35] as well as the orbital [36, 37] and spin Edelstein effects [38–41] were studied [33].

Figures 2(a-d) show the Fermi-energy dependence of the SAC. See Sec. IV B for computational details. In this

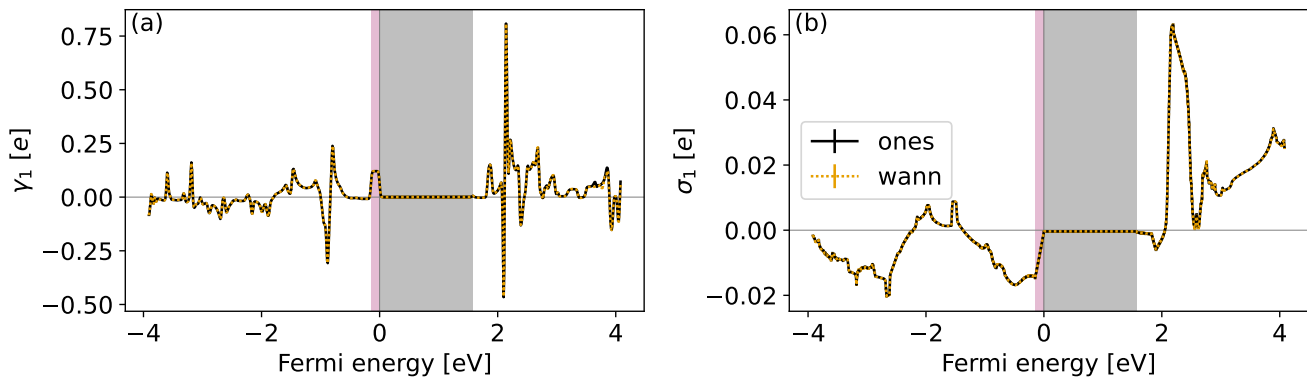


FIG. 1. (a) SAC $\gamma_1 = \epsilon^{1a}_{ij}\gamma_{sa}^{ij}/2$ and (b) SH conductivity $\sigma_1 = \epsilon^{1a}_{ij}\sigma_{sa}^{ij}/2$ per layer of monolayer MoS₂ as a function of the Fermi energy. Errors are defined by $\max_{\epsilon_1 \neq 0} |\gamma_{sa}^{ij} - \gamma_1|$ etc. Black solid and orange dotted lines correspond to the number of iterations for wannierization = 0 and 1,000, respectively. Gray and purple areas represent the band gap and the spin splitting at K and K' points owing to the Ising SOC, respectively.

material, the D_3 point group symmetry allows the form of

$$\gamma_{sa}^{ij} = \sum_{\alpha=1}^4 \gamma_{\alpha} \epsilon_{\alpha a}^{ij}, \quad (8)$$

in which $\epsilon_{\alpha a}^{ij}$ ($\alpha = 1, \dots, 4$) are tensors whose nonzero components are $\epsilon_{1z}^{xy} = -\epsilon_{1z}^{yx} = 1$, $\epsilon_{2x}^{xx} = -\epsilon_{2x}^{yy} = -\epsilon_{2y}^{xy} = -\epsilon_{2y}^{yx} = 1$, $\epsilon_{3x}^{yz} = -\epsilon_{3y}^{xz} = 1$, and $\epsilon_{4y}^{zx} = -\epsilon_{4x}^{zy} = 1$. Our results are consistent with the symmetry and gauge invariant, which validates our implementation.

In Figs. 2(e-h), we show the Fermi-energy dependences of the SH conductivities σ_{α} of the conventional spin current, which are defined similarly to Eq. (8). In the band gap painted in gray, we find $\sigma_{\alpha} = (-15, -2, -24, -4)$ (\hbar/e)S/cm. One of the critical problems in the SH conductivity is that it can be nonzero in insulators even though the spin accumulation does not occur. On the other hand, the SAC always vanishes in insulators because it is a Fermi-surface term as in Eq. (1).

III. DISCUSSION AND SUMMARY

A. Relevance of SAC

To clarify the relevance of the SAC as an indicator of the SH effect, let us summarize critical problems in the conventional spin current here. First, the equilibrium expectation value can be nonzero in the absence of the inversion symmetry [42]. This point is in a sharp contrast to the charge current, whose equilibrium expectation value is forbidden by the Bloch-Bohm theorem [43] even in the absence of the inversion and time-reversal symmetries. Second, there is no conjugate force, and hence Onsager's reciprocity does not hold. Finally, as

pointed out above, the SH conductivity can be nonzero in insulators, where the charge current does not flow and the spin accumulation is forbidden by the time-reversal symmetry. The conventional spin current describes neither transport phenomena nor the spin accumulation.

The conserved spin current [8] has some desirable properties. First, the equilibrium expectation value takes the form of a magnetization current, and hence the net equilibrium current vanishes, if the spin torque quadrupole moment is considered [44]. Second, this current is conjugate to the Zeeman field gradient, and Onsager's reciprocity holds [8]. Thus, the first and second problems in the conventional spin current have been resolved. In spite of these properties, it has not been proved yet that the conserved spin current is experimentally observed. Regarding the third problem, the SH conductivity remains nonzero in insulators [9]. Note that the formula in Ref. [9], which was based on Ref. [45], does not take the spin torque quadrupole moment and differs from that in Ref. [44].

The SAC are free from the aforementioned problems. First, it does not matter if the equilibrium expectation value of spin does not vanish. Second, Onsager's reciprocity holds [26]; the inverse SH effect can be characterized by the response of the charge current to the time derivative of the Zeeman field gradient. Finally, the SAC itself vanishes in insulators as seen in Eq. (1). Furthermore, the exponential decay of the spin accumulation can be reproduced if the diffusion propagator is taken into account [24], as discussed more in Sec. III B.

B. Limitations of SAC

We also comments on some limitations of the SAC. First, we rely on the relaxation time approximation and neglect the vertex corrections. Regarding the SH conductivity, the vertex corrections were taken into account in

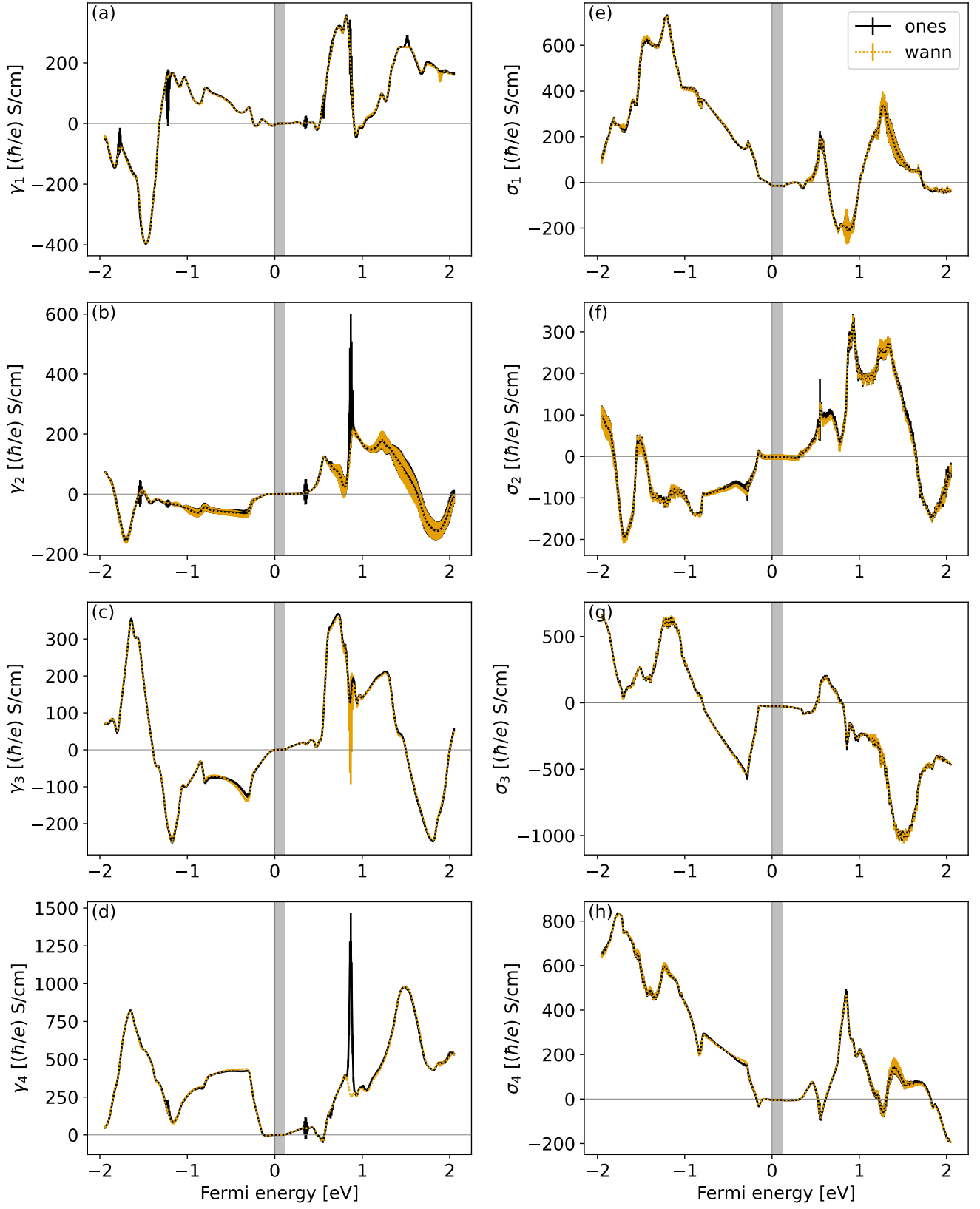


FIG. 2. (a-d) SAC $\gamma_\alpha = \epsilon^{\alpha a} \gamma_{sa}^{ij} / n_\alpha$ and (e-h) SH conductivity $\sigma_\alpha = \epsilon^{\alpha a} \sigma_{sa}^{ij} / n_\alpha$ of trigonal tellurium as a function of the Fermi energy, in which $n_\alpha = (2, 4, 2, 2)$ are the numbers of nonzero components in $\epsilon^{\alpha a}_{ij}$. Errors are defined by $\max_{\epsilon_\alpha \neq 0} |\gamma_{sa}^{ij} - \gamma_\alpha|$ etc. Black solid and orange dotted lines correspond to the number of iterations for wannierization = 0 and 1,000, respectively. Gray area represents the band gap.

alloy systems using the Korringa-Kohn-Rostoker method with the coherent potential approximation [46]. It is a future problem to evaluate the SAC based on the Green's functions [26] in the same manner.

Second, we neglect the effect of diffusion. Since the electric field gradient $\partial_{x^i} E_j$ has δ -function peaks at the surface, the induced spin density $\langle \Delta \hat{s}_a \rangle$ as well. If we take the diffusion propagator into account, the response becomes nonlocal, and the exponential decay can be reproduced [24]. To see this, let us consider to apply a uniform electric field E_{j0} to a finite section $-L/2 < x^i < L/2$. In the reciprocal space, the electric field is expressed by $E_j(Q_i) = (2E_{j0}/Q_i) \sin Q_i L/2$. Here we introduce the phenomenological diffusion factor $D_s(Q_i) = D_{s0}/[(Q_i l_s)^2 + 1]$, and the response is expressed by

$$\langle \Delta \hat{s}_a \rangle(Q_i) = D_s(Q_i) g_{sa}^{ij} Q_i E_j(Q_i). \quad (9)$$

D_{s0} and the spin diffusion length l_s depend on the details of disorder. Back to the real space, the spin density turns out to decay exponentially as

$$\langle \Delta \hat{s}_a \rangle(x^i) = \frac{D_{s0} g_{sa}^{ij}}{2l_s} E_{j0} \times (e^{-|x^i + L/2|/l_s} - e^{-|x^i - L/2|/l_s}). \quad (10)$$

Thus, the SAC g_{sa}^{ij} plays a crucial role in the spin accumulation.

Third, we neglect the surface effects because our scope is the spin accumulation from the bulk SH effect. Since the inversion symmetry is broken at the surface, the resulting Rashba SOC may cause the additional spin relaxation and the spin Edelstein effect [38–41]. Also, in topological insulators that are gapped in the bulk [47], the SAC vanishes, but the spin injection was experimentally succeeded [48]. This spin injection originates from the spin Edelstein effect owing to gapless surface states.

Finally, we neglect the intrinsic Fermi-sea term allowed in the absence of the time-reversal symmetry. Although this term is related to the magnetic SH effect experimentally observed recently [49], its explicit formula using Bloch wavefunctions has not been derived yet.

To summarize, we have developed an *ab initio* computational scheme for the SAC (1) that characterizes the spin accumulation owing to the SH effect as a bulk property. Using maximally localized Wannier functions, we can evaluate the SAC with dense \mathbf{k} -mesh for real materials. We have applied our method to monolayer TMDC MoS₂ and trigonal tellurium and checked the consistency with the point group symmetry and the gauge invariance as expected from the trace formula (3). We believe that the SAC is an alternative indicator of the SH effect without any ambiguity, and its Wannier interpolation would pave the way to quantitative materials research on the SH effect.

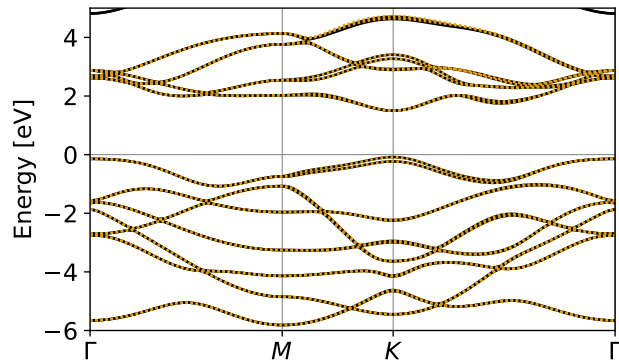


FIG. 3. Band structure of monolayer MoS₂ obtained by VASP (black solid line) and Wannier90 (orange square).

IV. METHODS

Our overall workflow is as follows. First, we carry out *ab initio* calculations with Vienna Ab initio Simulation Package (VASP) based on the projector augmented wave (PAW) method [50, 51]. The SOC is taken into account. Next, we construct Wannier functions with Wannier90 [28]. We also generate additional input files `seedname.uHu`, `spn`, `sIu` from VASP output files via WannierBerri [52]. Finally, we compute the SAC and SH conductivity [53] using a post-process code of Wannier90, `postw90`.

A. Computational details for monolayer MoS₂

Monolayer MoS₂, made from 2H-MoS₂, belongs to the space group No. 187 (D_{3h}^1 , $P6m2$). The lattice constants are not optimized from 2H-MoS₂ in Materials Project [54] No. 2815 and set to $a = 3.19$ Å and $c = 13.38$ Å, while the position of sulfur is optimized to the Wyckoff position $2h$ with $z = 0.116818$. In order to deal with the vdW interaction, we use rev-vdW-DF2 for the exchange correlation functional [55, 56]. We set the plain-wave energy cutoff to 258.689 eV and \mathbf{k} -mesh to $48 \times 48 \times 2$.

In Wannier90 calculations, we set the initial guess to d orbitals of molybdenum and p orbitals of sulfur, which leads to 22 Wannier functions, \mathbf{k} -mesh to $12 \times 12 \times 1$, the lower bound of the outer window to -6 eV measured from the Fermi energy, the inner window to $[-6$ eV, 4 eV], and the number of iterations for wannierization to 0 or 1,000. The total Wannier spread is reduced from 36.157 Å² to 35.881 Å². The obtained band structure is shown in Fig. 3.

In `postw90` calculations, we set the smearing to 0.02 eV and \mathbf{k} -mesh to $512 \times 512 \times 1$. The SAC and SH conductivity per layer in Fig. 1 are obtained by multiplying the c -axis length.

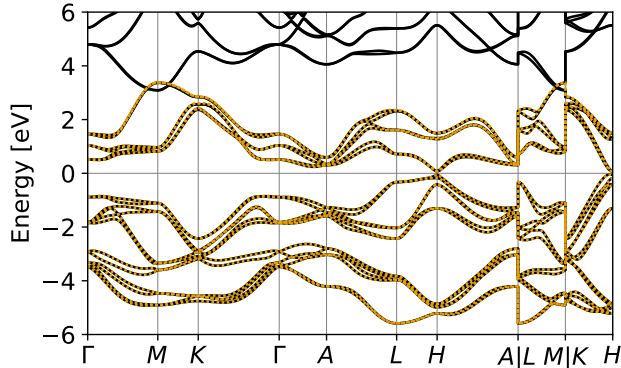


FIG. 4. Band structure of trigonal tellurium obtained by VASP (black solid line) and Wannier90 (orange square).

B. Computational details for trigonal tellurium

Trigonal tellurium is one of the most famous chiral materials belonging to the space group No. 152 (D_3^4 , $P3_121$). We do not carry out structural optimization and set the lattice constants to $a = 4.60$ Å and $c = 5.90$ Å in Materials Project [54] No. 19. Tellurium is located at the Wyckoff position $3a$ with $x = 0.256697$. We use the generalized gradient approximation proposed by Perdew, Burke, and Ernzerhof for the exchange correlation functional [57, 58]. We set the plain-wave energy cutoff to 174.982 eV and \mathbf{k} -mesh to $24 \times 24 \times 24$.

In Wannier90 calculations, we set the initial guess to p orbitals, which leads to 18 Wannier functions, \mathbf{k} -mesh to $6 \times 6 \times 6$, the inner window to $[-6$ eV, 2 eV] measured from the Fermi energy, and the number of iterations for wannierization to 0 or 1,000. The total Wannier spread

is reduced from 50.186 Å² to 50.048 Å². The obtained band structure is shown in Fig. 4.

In `postw90` calculations, we set the smearing to 0.02 eV and \mathbf{k} -mesh to $256 \times 256 \times 256$.

DATA AVAILABILITY

The data generated in this work will be made available upon reasonable request to the first author.

CODE AVAILABILITY

The code used to generate the results in this work will be made available upon reasonable request to the first author.

ACKNOWLEDGMENTS

We thank R. Arita and T. Koretsune for their advice on Wannier90. This work was supported by the Japan Society for the Promotion of Science KAKENHI (Grants No. JP22K03498 and No. JP23K21081).

AUTHOR CONTRIBUTIONS

A.S. developed the theory, implemented the code, and carried out calculations. A.S. and E.M. wrote the manuscript.

COMPETING INTERESTS

We declare no competing interests.

-
- [1] J. Sinova, S. O. Valenzuela, J. Wunderlich, C. H. Back, and T. Jungwirth, *Rev. Mod. Phys.* **87**, 1213 (2015).
 - [2] Y. K. Kato, R. C. Myers, A. C. Gossard, and D. D. Awschalom, *Science* **306**, 1910 (2004).
 - [3] J. Wunderlich, B. Kaestner, J. Sinova, and T. Jungwirth, *Phys. Rev. Lett.* **94**, 047204 (2005).
 - [4] S. Shi, X. Wang, Y. Zhao, and W. Zhao, *Mater. Today Elec.* **6**, 100060 (2023).
 - [5] V. Baltz, A. Manchon, M. Tsoi, T. Moriyama, T. Ono, and Y. Tserkovnyak, *Rev. Mod. Phys.* **90**, 015005 (2018).
 - [6] G. Y. Guo, Y. Yao, and Q. Niu, *Phys. Rev. Lett.* **94**, 226601 (2005).
 - [7] Y. Yao and Z. Fang, *Phys. Rev. Lett.* **95**, 156601 (2005).
 - [8] J. Shi, P. Zhang, D. Xiao, and Q. Niu, *Phys. Rev. Lett.* **96**, 076604 (2006).
 - [9] H. Ma, J. H. Cullen, S. Monir, R. Rahman, and D. Culcer, *npj Spintronics* **2**, 55 (2024).
 - [10] E. G. Mishchenko, A. V. Shytov, and B. I. Halperin, *Phys. Rev. Lett.* **93**, 226602 (2004).
 - [11] X. Ma, L. Hu, R. Tao, and S.-Q. Shen, *Phys. Rev. B* **70**, 195343 (2004).
 - [12] E. I. Rashba, *Physica E* **34**, 31 (2006).
 - [13] R. Raimondi, C. Gorini, P. Schwab, and M. Dzierzawa, *Phys. Rev. B* **74**, 035340 (2006).
 - [14] B. K. Nikolić, S. Souma, L. P. Zárbo, and J. Sinova, *Phys. Rev. Lett.* **95**, 046601 (2005).
 - [15] M. Onoda and N. Nagaosa, *Phys. Rev. B* **72**, 081301(R) (2005).
 - [16] B. K. Nikolić, L. P. Zárbo, and S. Souma, *Phys. Rev. B* **73**, 075303 (2006).
 - [17] J.-i. Inoue, G. E. W. Bauer, and L. W. Molenkamp, *Phys. Rev. B* **70**, 041303(R) (2004).
 - [18] R. Raimondi and P. Schwab, *Phys. Rev. B* **71**, 033311 (2005).
 - [19] O. Chalaev and D. Loss, *Phys. Rev. B* **71**, 245318 (2005).
 - [20] O. Chalaev and D. Loss, *Phys. Rev. B* **73**, 049901(E) (2006).
 - [21] O. V. Dimitrova, *Phys. Rev. B* **71**, 245327 (2005).
 - [22] A. Khaetskii, *Phys. Rev. Lett.* **96**, 056602 (2006).

- [23] N. Sugimoto, S. Onoda, S. Murakami, and N. Nagaosa, *Phys. Rev. B* **73**, 113305 (2006).
- [24] G. Tatara, *Phys. Rev. B* **98**, 174422 (2018).
- [25] A. Shitade and G. Tatara, *Phys. Rev. B* **105**, L201202 (2022).
- [26] A. Shitade, *Phys. Rev. B* **106**, 045203 (2022).
- [27] N. Marzari, A. A. Mostofi, J. R. Yates, I. Souza, and D. Vanderbilt, *Rev. Mod. Phys.* **84**, 1419 (2012).
- [28] G. Pizzi, V. Vitale, R. Arita, S. Blügel, F. Freimuth, G. Géranton, M. Gibertini, D. Gresch, C. Johnson, T. Koretsune, J. Ibañez-Azpiroz, H. Lee, J.-M. Lihm, D. Marchand, A. Marrazzo, Y. Mokrousov, J. I. Mustafa, Y. Nohara, Y. Nomura, L. Paulatto, S. Poncé, T. Ponweiser, J. Qiao, F. Thöle, S. S. Tsirkin, M. Wierzbowska, N. Marzari, D. Vanderbilt, I. Souza, A. A. Mostofi, and J. R. Yates, *J. Phys.: Condens. Matter* **32**, 165902 (2020).
- [29] A. Shitade, A. Daido, and Y. Yanase, *Phys. Rev. B* **99**, 024404 (2019).
- [30] D. Xiao, J. Shi, and Q. Niu, *Phys. Rev. Lett.* **95**, 137204 (2005).
- [31] D. Xiao, J. Shi, and Q. Niu, *Phys. Rev. Lett.* **95**, 169903(E) (2005).
- [32] M. G. Lopez, D. Vanderbilt, T. Thonhauser, and I. Souza, *Phys. Rev. B* **85**, 014435 (2012).
- [33] S. S. Tsirkin, P. A. Puente, and I. Souza, *Phys. Rev. B* **97**, 035158 (2018).
- [34] W. Feng, Y. Yao, W. Zhu, J. Zhou, W. Yao, and D. Xiao, *Phys. Rev. B* **86**, 165108 (2012).
- [35] I. Sodemann and L. Fu, *Phys. Rev. Lett.* **115**, 216806 (2015).
- [36] J. Ma and D. A. Pesin, *Phys. Rev. B* **92**, 235205 (2015).
- [37] S. Zhong, J. E. Moore, and I. Souza, *Phys. Rev. Lett.* **116**, 077201 (2016).
- [38] E. L. Ivchenko and G. E. Pikus, *Pis'ma Zh. Eksp. Teor. Fiz.* **27**, 640 (1978), [*JETP Lett.* **27**, 604–608 (1978)].
- [39] E. L. Ivchenko, Y. B. Lyanda-Geller, and G. E. Pikus, *Pis'ma Zh. Eksp. Teor. Fiz.* **50**, 156 (1989), [*JETP Lett.* **50**, 175–177 (1989)].
- [40] A. G. Aronov and Y. B. Lyanda-Geller, *Pis'ma Zh. Eksp. Teor. Fiz.* **50**, 398 (1989), [*JETP Lett.* **50**, 431–434 (1989)].
- [41] V. M. Edelstein, *Solid State Commun.* **73**, 233 (1990).
- [42] E. I. Rashba, *Phys. Rev. B* **68**, 241315(R) (2003).
- [43] D. Bohm, *Phys. Rev.* **75**, 502 (1949).
- [44] C. Xiao and Q. Niu, *Phys. Rev. B* **104**, L241411 (2021).
- [45] H. Liu, J. H. Cullen, and D. Culcer, *Phys. Rev. B* **108**, 195434 (2023).
- [46] S. Lowitzer, M. Gradhand, D. Ködderitzsch, D. V. Fedorov, I. Mertig, and H. Ebert, *Phys. Rev. Lett.* **106**, 056601 (2011).
- [47] M. Z. Hasan and C. L. Kane, *Rev. Mod. Phys.* **82**, 3045 (2010).
- [48] Y. Shiomi, K. Nomura, Y. Kajiwara, K. Eto, M. Novak, K. Segawa, Y. Ando, and E. Saitoh, *Phys. Rev. Lett.* **113**, 196601 (2014).
- [49] M. Kimata, H. Chen, K. Kondou, S. Sugimoto, P. K. Muduli, M. Ikhlas, Y. Omori, T. Tomita, A. H. MacDonald, S. Nakatsuji, and Y. Otani, *Nature (London)* **565**, 627 (2019).
- [50] G. Kresse and J. Furthmüller, *Phys. Rev. B* **54**, 11169 (1996).
- [51] G. Kresse and D. Joubert, *Phys. Rev. B* **59**, 1758 (1999).
- [52] S. S. Tsirkin, *npj Comput. Mater.* **7**, 33 (2021).
- [53] J. H. Ryoo, C.-H. Park, and I. Souza, *Phys. Rev. B* **99**, 235113 (2019).
- [54] A. Jain, S. P. Ong, G. Hautier, W. Chen, W. D. Richards, S. Dacek, S. Cholia, D. Gunter, D. Skinner, G. Ceder, and K. A. Persson, *APL Mater.* **1**, 011002 (2013).
- [55] I. Hamada, *Phys. Rev. B* **89**, 121103 (2014).
- [56] I. Hamada, *Phys. Rev. B* **91**, 119902(E) (2015).
- [57] J. P. Perdew, K. Burke, and M. Ernzerhof, *Phys. Rev. Lett.* **77**, 3865 (1996).
- [58] J. P. Perdew, K. Burke, and M. Ernzerhof, *Phys. Rev. Lett.* **78**, 1396 (1997).